6.
SHARED RADIATOR MIMO ANTENNA

6.1 Introduction

As discussed in previous chapter, the UWB antenna used in MIMO systems combined with MIMO technology can handle high data rate signals with minimal multipath fading, since MIMO systems employ multiple antennas, which transmit/receive multiple spatial signals with different fading characteristics at the same time. It is very much unlikely that all received signals are influenced by deep fading. Thus, the system reliability in terms of minimal multipath fading can be enhanced through appropriate selection of received signals. One of the major hurdles in the design of MIMO antenna is to maintain high isolation between antenna ports over its operating bandwidth. In past few years, the design and development of compact MIMO antenna using planar UWB antennas have grown rapidly. In the early phase, planar monopole antennas (PMA) operating in orthogonal polarizations were proposed for UWB MIMO applications. The orthogonal polarization configuration is achieved by placing multiple PMAs perpendicular to each other. In reference [Liu *et al.* (2013)], two long ground stubs acting as parasitic monopoles were used to isolate two rectangular-shaped PMAs placed in orthogonal arrangement, whereas a long slot on ground was used for obtaining proper isolation between two orthogonally arranged PMAs [Ren *et al.* (2014)]. Further, single long stub was utilized to isolate two octagonal-shaped PMAs having Koch fractal geometry on their edges [Tripathi *et al.* (2015)]. Similarly, in reference [Gao *et al.* (2014)], isolation is achieved through a long stub placed symmetrically (at 45^0) between two staircase-shaped radiating elements kept orthogonally. However, a kind of multimode resonator (MMR) was appended to get proper isolation between four orthogonally arranged circular PMAs [Kiem *et al.* (2014)]. Subsequently, in reference [Huang *et al.* (2014)], a MIMO antenna arrangement is described in which two- and four-PMAs are placed in orthogonal polarization and they are well isolated from each other without using extra isolation technique. This type of perpendicular arrangement

isolates antenna ports with/without use of a stub or slot but increases the overall antenna size. To reduce overall size, the PMAs can be placed side-by-side instead of placing them in perpendicular arrangement. But side-by-side arrangement of PMAs decreases isolation between antenna ports. Therefore, need was felt to improve isolation between antenna ports through introduction of extra isolation mechanism in the system. Keeping this aspect in view, two UWB MIMO antennas using half circular disk monopole antenna elements and half square monopole antenna elements arranged in side-by-side configurations were designed [Zhao *et al*. (2014)]. A vertical stub attached to ground plane is placed in between the antenna elements for maintaining proper isolation between antenna ports. In literature, different isolation enhancement mechanisms have been devised which include the use of strips beneath the patches [Khan *et al*. (2015)], parasitic decoupling elements [Tang *et al.* (2014)], T-shaped ground stub along with slot [Liu *et al.* (2015)], electromagnetic band gap (EBG) structure [Li *et al.* (2015)], comb-line structure [Malekpour *et al.* (2015)] in between the PMAs that are placed side-by-side to each other. Further, the quasi-self-complementary antenna (QSCA) elements arranged side-by-side without any extra isolation technique is also reported to form broadband MIMO antenna [Liu *et al.* (2014)]. Furthermore, a MIMO antenna using two-elements of castor leaf-shaped QSCA with and without dual band-rejection characteristics is described in previous chapter.

In the recent past, common radiator operating in dual polarization was utilized as a two-port UWB MIMO antenna [Mao *et al.* (2014)]. The requirement for maintaining high isolation between antenna ports increases for compact MIMO antenna system utilizing shared radiating patch. One of the solutions to obtain adequate isolation between antenna ports is the use of slot in the shared radiator. In reference [Mao *et al.* (2014)], high isolation is reported using the combination of T-shaped slot on patch, a pair of slits on ground plane and a stub attached to ground plane. In reference [Zhang *et al.* (2015)], a compact UWB MIMO antenna is proposed using a shared radiator fed by two asymmetrical-coplanar-strip (ACS) lines and isolation is achieved with the help of an I-shaped slot in radiator, a stub attached to ground plane, a slot on ground plane, and a

parasitic strip on back of antenna substrate. Further, a circular patch is shared by two coplanar waveguide (CPW) feeds and isolation is obtained through a single slot in patch the [Srivastava *et al.* (2016)], combination of slot in patch and stub attached to ground plane [Srivastava *et al.* (2015)]. Srivastava *et al.* (2015) obtained two band-rejections using elliptical split ring slots. Furthermore, Khan *et al.* (2016) maintained good isolation using only a cross-shaped slot inserted in a shared radiator, but antenna performance is not identical for both ports due to asymmetrical radiator configuration seen from the-two ports. In addition, most of the shared radiators are reported for UWB MIMO applications and use slots in radiator patch for obtaining adequate isolation between antenna ports.

In this chapter, a broadband MIMO antenna using a shared radiator is proposed in which good isolation between antenna ports is achieved without introducing any slot in the patch. The proposed antenna comprises of a modified leaf-shaped radiating element shared symmetrically at 45^0 by two tapered microstrip lines and a common curved ground plane. Adequate isolation between antenna ports over its operating frequency band is obtained through the utilization of end-loaded meandered line attached to modified curved ground plane. The proposed antenna is 39×39 mm^2 in size and provides simulated -10 dB reflection coefficient bandwidth of 10.35 GHz (136.63 %) over the frequency range 2.4−12.75 GHz with reasonable $S_{21} \leq$ -15 dB over its operating frequency band. The designed antenna was fabricated and measurement of its input, mutual coupling and radiation characteristics was made over its whole operating frequency range. Further, measured results are compared with the respective simulation results obtained through simulation using Computer Simulation Technology Microwave Studio (CST MWS) software.

6.2 Design and Configuration of Shared Radiator MIMO Antenna

Figure 6.1 shows the geometrical configuration of proposed two-port MIMO antenna along with its dimensional parameters. The proposed antenna consists of single leaf-shaped radiating patch, which is shared by two tapered microstrip lines on the top side of cost effective FR4 substrate having thickness of

0.8 mm and relative permittivity of 4.4. An end-loaded meandered line stub is attached to supporting curved ground plane on the bottom side of the substrate (bottom-side). The whole geometry of antenna is symmetrical about a line drawn at an angle of -45^0 from Y-axis which results in identical performance of the antenna from either port. The tapered microstrip line is utilized for proper impedance matching between 50 Ω coaxial feed and the antenna. Two ports of the proposed MIMO antenna uses single radiator instead of two, thereby reducing overall size of the antenna as compared to conventional MIMO antenna system having two identical antenna elements placed in orthogonal or side-by-side arrangement. Due to the shared radiator and compact size of the proposed antenna in absence of ground plane stub, mutual coupling between antenna ports increases. The mutual coupling between antenna ports is reduced by attaching a metallic stub to the ground plane. The length of the stub is increased through the use of meander line and pentagonal patch at the end of stub so that isolation can be increased for lower operating frequencies. Apart from the stub, the length of ground plane is increased by creating slot in the ground plane where stub is attached, and by making the outer boundaries of ground plane curved.

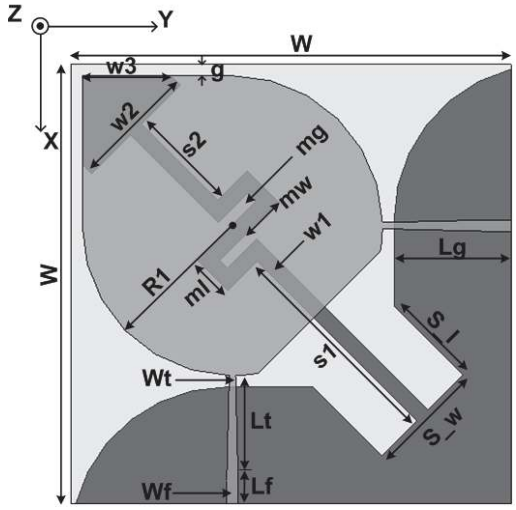

Figure 6.1: Geometrical configuration of proposed shared radiator MIMO antenna.

The configurations resulting from different stages of antenna design are shown in Figure 6.2. The optimized values of dimensional parameters of the

proposed antenna obtained through simulation using Computer Simulation Technology Microwave Studio (CST MWS) software are listed in Table 6.1.

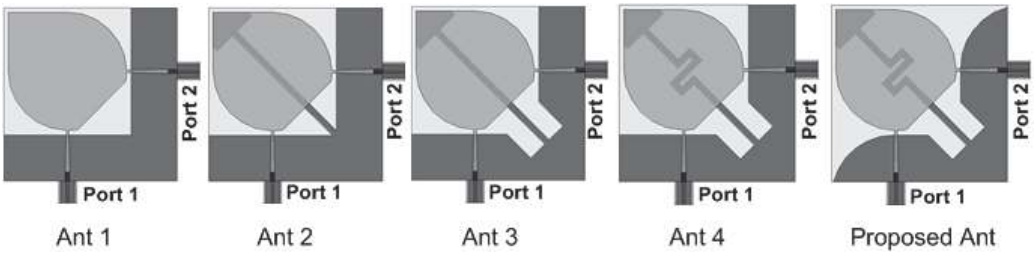

Figure 6.2: Evolution steps of the proposed antenna.

Table 6.1: Design parameters of the proposed shared radiator MIMO antenna

Parameter	Value (mm)	Parameter	Value (mm)
W	39	R1	13.3
Lf	2	s1	22.2
Lt	9.4	s2	7
Wf	1	w1	1.4
Wt	0.3	w2	11
Lg	10.4	w3	7.78
S_l	8.5	ml	3.8
S_w	11	mw	4.3
g	1	mg	1

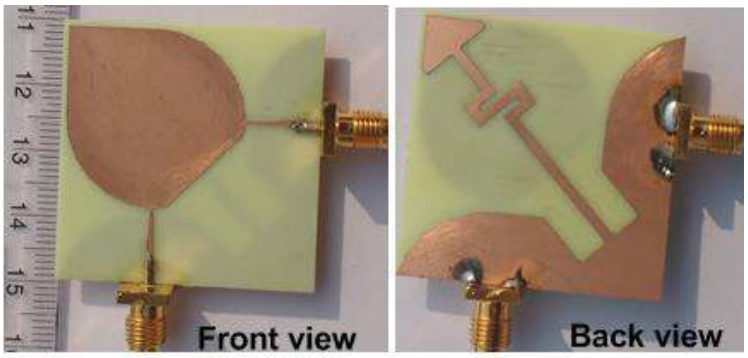

(a) (b)

Figure 6.3: Prototype of fabricated antenna (a) front view and (b) back view.

6.3 Simulation and Experimental Studies

6.3.1 *Simulation Study*

The simulation study of the proposed shared radiator MIMO antenna was carried out using Computer Simulation Technology Microwave Studio (CST

MWS) software. Five different MIMO antenna configurations were considered starting from basic configuration (Ant 1) consisting of leaf-shaped patch and rectangular ground plane. The fifth configuration i.e. the proposed antenna configuration and its optimum dimensions were found through gradual modification in the basic antenna configuration (Ant 1) to obtain improved simulated S-parameters-frequency characteristics over broad bandwidth when exciting port 1. The proposed antenna with optimum dimensions (given in Table 6.1 was then used to obtain its simulated input, radiation and diversity performance characteristics. The simulated S-parameter-frequency characteristics of different antenna configurations and desired input, mutual coupling, radiation and diversity characteristics of the proposed antenna were obtained through simulation.

6.3.2 *Experimental Study*

The proposed MIMO antenna with optimum dimensions was fabricated using T-Tech QC5000 Quick Circuit prototyping machine. The photographs of fabricated antenna are shown in Figure 6.3. The fabricated antenna was tested experimentally. The S-parameter-frequency characteristics of the antenna were measured using Anritsu make VNA Master Vector Network Analyzer (Model: MS2038C). The two-dimensional (2D) radiation patterns of the proposed MIMO antenna with port 1 excited and port 2 match terminated with 50 Ω load were measured in an anechoic chamber at discrete frequencies over its operating frequency range. For measuring the radiation patterns of the proposed antenna, 1−18 GHz broadband horn antenna was used as transmitting (Tx) antenna and the proposed antenna acting as receiving (Rx), antenna which was placed in the far-field region inside the anechoic chamber was rotated along its own axis in H- and E-planes using the antenna positioner system. The input port of transmitting horn and the output port of receiving antenna (the proposed antenna) were connected respectively to ports 1 and 2 of Agilent make ENA series Vector Network Analyzer (Model: E5071C) to measure the magnitudes of scattering parameter $|S'_{21}|$ (transmission coefficient from transmitting antenna to receiving antenna output) at different angles for the given plane and frequency of interest.

The gain values of the antenna are found using Friis formula (equation 6.1 or 6.2) utilizing same setup as used for measurement of radiation patterns of the proposed antenna.

$$P_R = \frac{P_T G_T G_R}{\left(\frac{4\pi R}{\lambda}\right)^2} \tag{6.1}$$

$$\frac{P_R}{P_T} = |S'_{21}|^2 = \frac{G_T G_R}{\left(\frac{4\pi R}{\lambda}\right)^2}$$

$$|S'_{21}|dB = 20log|S'_{21}| = (G_T)dB + (G_R)dB + 20log\left(\frac{\lambda}{4\pi R}\right) \tag{6.2}$$

where $|S'_{21}|^2$ is the ratio of the received power 'P_R' to the transmitted power 'P_T', G_T and G_R are the power gains of Tx and Rx antennas respectively, R is distance between them and λ is the operating wavelength. Losses in the coaxial cables used on the transmitting and receiving sides were also taken into account while using the Friis formula to calculate the gain 'G_R' of the proposed antenna at the frequency of interest. However, the values of realized gain (G'_R) are calculated using equation (6.3).

$$G'_R = (G_R)dB + 10log\,(1 - |S_{11}|^2) \tag{6.3}$$

where S_{11} is reflection coefficient at antenna port 1.

Further, the total efficiency measurement was performed using Wheeler cap method as explained in previous chapter. Equation (6.4) was used to determine total efficiency 'η_T' of the proposed antenna from the measured parameters.

$$\eta_T = (1 - |S_{11FS}|^2)\sqrt{\frac{|S_{11WC}|^2 - |S_{11FS}|^2}{1 - 2|S_{11FS}|^2 + |S_{11FS}|^2|S_{11WC}|^2}} \tag{6.4}$$

where S_{11FS} and S_{11WC} are the values of reflection coefficient of the proposed antenna when the antenna was placed in free space and inside the Wheeler cap respectively.

Further, experimental values of envelope correlation coefficient (ECC) were obtained from measured S-parameters using equation (6.5).

$$ECC = \frac{|S_{11}^{*}S_{12}+S_{21}^{*}S_{22}|^{2}}{(1-(|S_{11}|^{2}+|S_{21}|^{2}))(1-(|S_{22}|^{2}+|S_{12}|^{2}))} \quad (6.5)$$

where S_{11} and S_{22} are the reflection coefficients at antenna ports 1 and 2 respectively, and S_{12} and S_{21} are the values of coupling from antenna ports 2 to 1 and ports 1 to 2 respectively.

Simulated and corresponding measured results for S-parameter-frequency characteristics, radiation patterns, realized gain-, total efficiency-frequency characteristic and variations of envelope correlation coefficient of the proposed antenna versus frequency are compared and discussed in different Sub-sections of the Results and Discussion Section.

6.4 Results and Discussion

6.4.1 *S-parameters-Frequency Characteristics*

6.4.1.1 Different Antenna Configurations

The S-parameters (S_{11} and S_{21})-frequency characteristics of various antenna configurations designated as Ant 1, Ant 2, Ant 3, Ant 4 and Proposed Ant in Figure 6.2 were studied through simulation when exciting port 1 in order to obtain improved input reflection coefficient and mutual coupling (S_{21}) characteristics for the final proposed antenna configuration over broad range of frequencies. The steps involved for isolation enhancement over broad range of frequency spectrum in going from Ant 1 to the Proposed Ant without disturbing patch geometry of the antenna are explained using S-parameter-frequency characteristics of different antenna configurations as shown in Figure 6.4. The S-parameters (S_{11} and S_{21})-frequency characteristics when exciting port 1 only are considered for different antenna configurations due to almost identical S-parameter-frequency characteristics when exciting either of the antenna ports as shown in Figure 6.5.

First configuration, ‘Ant 1’ pertains to shared radiator MIMO antenna consisting of single leaf-shaped radiating patch with rectangular ground plane without any modification. It is observed from Figure 6.4(a) that the ‘Ant 1’ provides S_{11} values ≤ -10 dB over wide range of frequencies while S_{21} is greater than or equal to -15 dB for most of the frequencies except the frequencies around

4.1 GHz as shown in Figure 6.4(b). The mutual coupling (S_{21}) between ports 1 and 2 of 'Ant 1' for most of the frequencies is relatively high because the path length (for current on surface of ground plane) between ports 1and 2 is less.

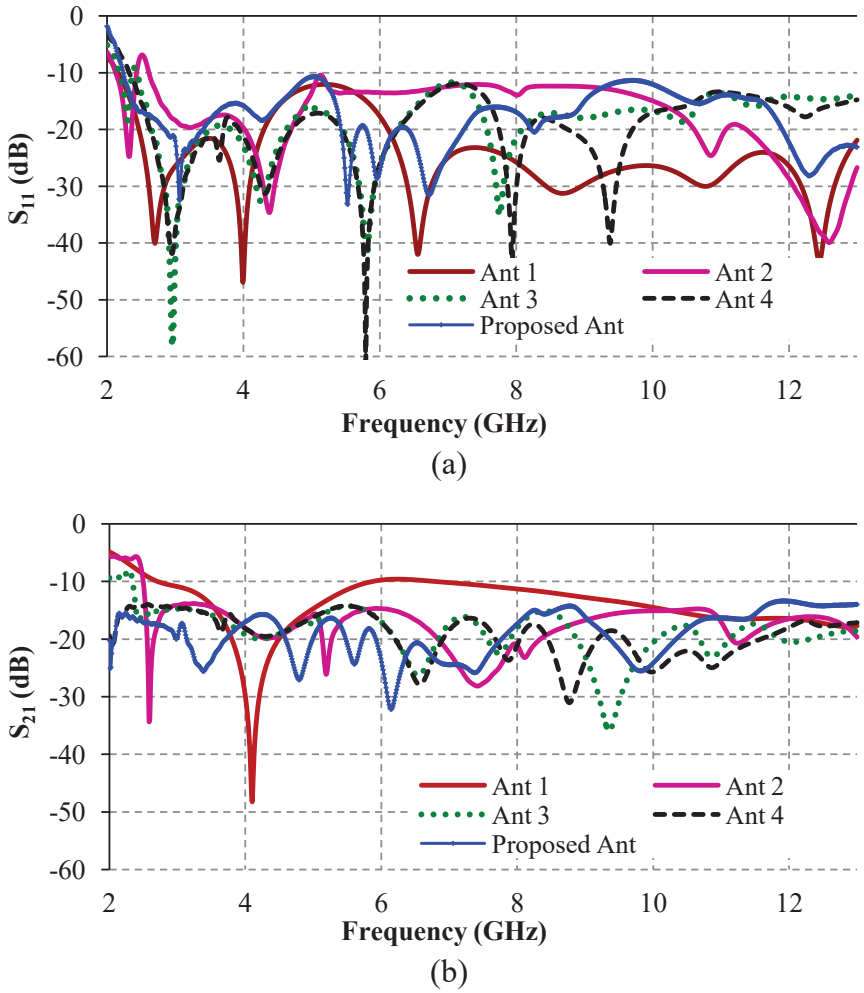

Figure 6.4: S-parameter-frequency characteristics of different antenna configurations when exciting port 1 (a) S_{11} and (b) S_{21}.

Therefore, in the second configuration specified as 'Ant 2', a top-loaded stub which is symmetrical about a line drawn at an angle of 45^0 with respect to X-axis is attached to ground plane to increase the path length. It can be observed that the 'Ant 2' provides reduced S_{21} values over broader frequency spectrum as compared to 'Ant 1' while reflection coefficient (S_{11}) values remain equal or below -10 dB over the frequency range 2.13−2.43 GHz and for frequencies more than 2.6 GHz. It is to be noted from Figure 6.4(b) that S_{21} values for 'Ant 2' have

gone down as compared to the values for ‘Ant 1’ but these values are not well below -15 dB.

In the third configuration specified as ‘Ant 3’, a rectangular slot is created on the ground plane where stub is attached. Slot on ground plane is arranged in such a manner that it further increases the path length between antenna ports. It is observed from Figure 6.4 that the ‘Ant 3’ provides much reduced values of S_{21} for lower and higher frequencies within the frequency range of interest as compared to ‘Ant 2’ whereas S_{11} values are maintained at or below -10 dB over the frequency range 2.16−2.37 GHz and for frequencies more than 2.44 GHz. But still possibility exists to further reduce the S_{21} values for lower frequencies.

In fourth configuration mentioned as ‘Ant 4’, the length of stub is increased by creating a meander line on stub. It can be further observed from Figure 6.4 that ‘Ant 4’ provides smaller S_{21} values towards lower frequencies while slight increase in lower cutoff frequency is obtained on the basis of S_{11}-frequency characteristic of ‘Ant 4’ as compared with ‘Ant 3’. It is found that the reduced S_{21} values towards lower frequency side are achieved due to the meander line stub which increases the path length (for current flow on ground plane) between antenna ports. Though S_{21} values of ‘Ant 4’ are reduced below -14 dB over wider operating frequency range but slight increase in lower cutoff frequency (at which S_{11} = -10 dB) of ‘Ant 4’ as compared with ‘Ant 3’ needs further investigation.

In the final configuration, that is, the Proposed Ant, the outer boundaries of ground plane are curved. It is observed from Figures 6.4(a) and (b) that Proposed Ant provides slightly reduced lower cutoff frequency as compared to ‘Ant 4’ whereas S_{21} values are further reduced for lower frequencies and maintained at or below -15 dB over whole of its operating frequency range. It is noted that the curved boundaries of ground plane help in smooth transition of current from feed line to patch as well as around the boundaries of ground plane.

Moreover, it is inferred through discussion on the variations of S_{21}-parameter with frequency for different antenna configurations that the modifications done on ground plane play a very important role in the isolation enhancement between two antenna ports.

6.4.1.2 Proposed Antenna Configuration

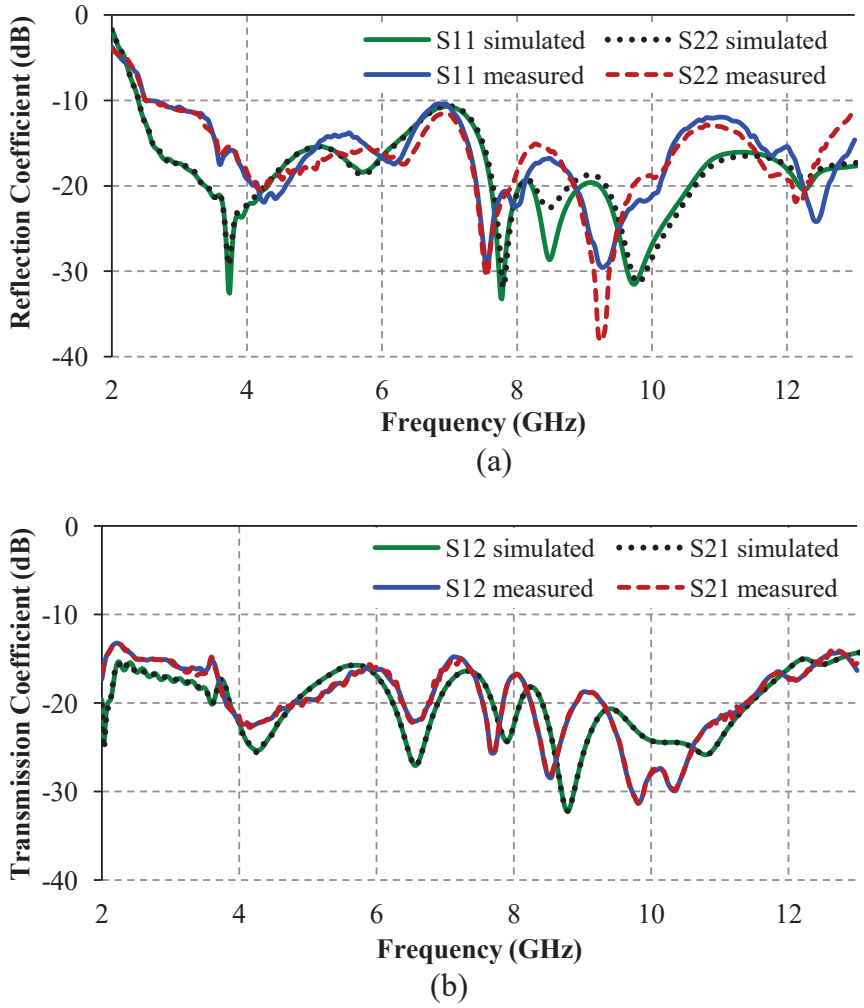

Figure 6.5: S-parameter-frequency characteristics of the proposed antenna (a) reflection coefficients S_{11} and S_{22} and (b) transmission coefficients S_{21} and S_{12}.

The variations of simulated and measured S-parameters (S_{11}, S_{21}, S_{12}, and S_{22}) of the proposed MIMO antenna with frequency are shown in Figure 6.5. Figures 6.5(a) and (b) depict the reflection and transmission coefficients-frequency characteristics respectively when exciting antenna ports (port 1/port 2) one at a time. It is clear from Figure 6.5 that respective simulated and measured S-

parameter-frequency characteristics of the antenna nearly match each other. It is also clear from Figure 6.5(a) that values of S_{11} and S_{22} are almost identical to each other except for frequencies of more than 7.5 GHz, whereas values of S_{21} and S_{12} (shown in Figure 6.5(b)) are identical over the whole operating frequency range of the antenna. The discrepancy between S_{11} and S_{22} values at different frequencies may arise because of the shape of meandered line which does not look symmetrical from both input ports of the antenna while S_{21}- and S_{12}- values are identical because length of meander line in terms of wavelength at any frequency of interest is same for both ports.

However, it is observed from Figure 6.5(a) that simulated reflection coefficient (S_{11} or S_{22}) values $\leq$ -10 dB for the proposed antenna are obtained for frequencies starting from 2.4 GHz while its measured reflection coefficient values remain less than or equal to -10 dB for frequencies starting from 2.5 GHz. Similarly, it is observed from Figure 6.5(b) that simulated and measured transmission coefficient (mutual coupling S_{21}/S_{12}) values $\leq$ -15 dB between antenna ports are obtained over frequency ranges 2.00−12.75 GHz and 2.50−12.45 GHz respectively. Therefore, it is found that the antenna provides simulated and measured bandwidths with respect to -10 dB reflection coefficient and -15 dB mutual coupling between ports of 5.3:1 (2.4−12.75 GHz) and 4.98:1 (2.5−12.45 GHz) respectively, which are nearly in agreement with each other. It is to be noted from Figure 6.5 that almost identical reflection coefficient-/ transmission coefficient- frequency characteristics of the proposed antenna are obtained when exciting either port of the antenna. This is the reason behind considering S_{11}- and S_{21}-frequency characteristics of different antenna configurations when exciting antenna port 1 only.

6.4.2 *Simulated Surface Current Distributions*

To better understand the influence of different antenna configurations (or the effect of different modifications done on ground plane) on isolation between antenna ports 1 and 2, the current distributions on the surfaces of different antenna configurations are discussed in this section. Figure 6.6 depicts the surface current

distributions for different antenna configurations when exciting port 1 at the frequencies of 2.5 and 6.0 GHz where S_{21} values are relatively higher for 'Ant 1' (first antenna configuration). It is to be noted that S_{21} value for 'Ant 1' is lowest among different antenna configurations at the frequency of 4.1 GHz. It can be clearly observed from Figure 6.6 that for 'Ant 1', higher levels of current are found near port 2 when exciting port 1 at frequencies of 2.5 and 6.0 GHz which indicates that mutual coupling between ports 1 and 2 of 'Ant 1' is high. It is also noticed that the higher level of current reaches port 2 from port 1 through ground plane. Therefore, to minimize the mutual coupling, a stub was attached to ground plane in 'Ant 2' as shown in Figure 6.2. The stub increases the path length between ports 1 and 2. Subsequently, it is observed that for 'Ant 2' level of surface current is reduced near port 2 at 6.0 GHz while it is higher in 'Ant 2' at 2.5 GHz as compared to 'Ant 1'. It is investigated from this observation that mutual coupling in 'Ant 2' reduces at higher frequencies due to the stub while it increases or remains higher for lower frequencies.

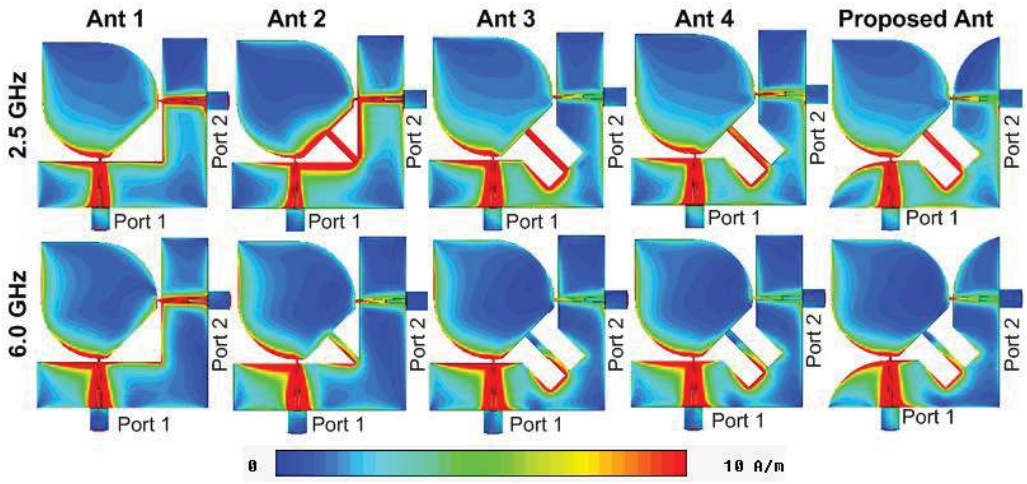

Figure 6.6: Simulated surface current distributions of different antenna configurations.

In order to minimize mutual coupling at lower frequencies too, a rectangular slot was created in the ground plane of 'Ant 2' which further increases the path length between the antenna ports and the resultant antenna configuration is designated as 'Ant 3'. It is noticeable that the levels of current near port 2 of 'Ant 3' are reduced at both frequencies of 2.5 and 6.0 GHz as compared to 'Ant

2'. This observation indicates that the combination of stub and slot reduces the mutual coupling for both higher as well as lower frequencies due to the increased path length between the antenna ports. The mutual coupling remains higher in 'Ant 3' for frequencies less than 2.4 GHz as can be seen from Figure 6.4. For this reason, the meander line stub is created and the resultant antenna configuration is designated as 'Ant 4' (shown in Figure 6.2). It can be observed that levels of current near port 2 of 'Ant 4' which is proportional to mutual coupling are still maintained at lower level at the frequencies of 2.5 and 6.0 GHz as shown in Figure 6.6. Mutual coupling is further reduced below -14 dB for frequencies less than 2.4 GHz (shown in Figure 6.4(b)) using meander line stub, which provides the increased path length as compared to 'Ant 3'.

To further reduce the mutual coupling below -15 dB for frequencies less than 2.4 GHz, the ground plane is curved from the corner and the resulting antenna configuration is designated as 'Proposed Ant'. It is observed from the surface current distribution on the 'Proposed Ant' that higher levels of current are smoothly distributed over the boundaries of ground plane near port 1 of the antenna whereas current distribution has lower levels near port 2 for frequencies of 2.5 and 6.0 GHz as compared to 'Ant 4'. Further, it is already observed from Figure 6.4(b) that S_{21} (mutual coupling) values of 'Proposed Ant' are reduced below -15 dB for frequencies lower than 2.5 GHz. It is investigated from aforesaid observations that the reduced mutual coupling for lower frequencies may be due to the smooth transition of current around the longer boundaries of curved ground plane which supports lower frequencies (higher wavelength) as compared to straight ground plane boundaries in 'Ant 4'.

6.4.3 *Radiation Patterns*

Figure 6.7 shows 3D radiation patterns in terms of realized gain of proposed MIMO antenna at 6 GHz when exciting port 1/2 while port 2/1 match-terminated with 50 Ω load. It is observed from Figure 6.7 that the radiation patterns are slightly directive towards upper boundary of patch near the excited port. When port 1 of the antenna is excited, maximum radiation occurs around -Y-

axis (around patch boundary near port 1) whereas when port 2 is excited maximum radiation occurs around -X-axis (around patch boundary near port 2). It is investigated through this observation that the radiation patterns for the excited ports 1 and 2 are mirror images of each other about a line drawn at an angle of 45^0 with respect to X-axis.

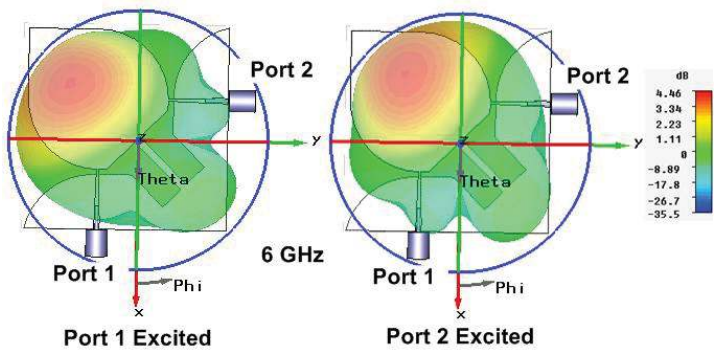

Figure 6.7: 3D radiation patterns of the proposed MIMO antenna when exciting port1/2 while match-terminating port 2/1.

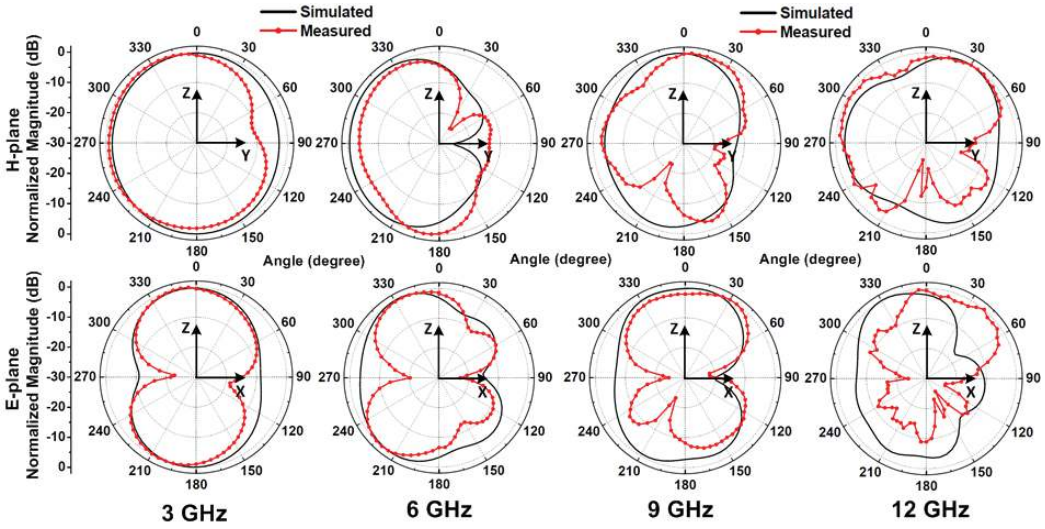

Figure 6.8: 2D radiation patterns of the proposed MIMO antenna when exciting port 1 while match-terminating port 2.

Owing to the symmetrical patterns, 2D radiation patterns are discussed with only one port excited and other port match-terminated. Figure 6.8 shows the simulated and measured normalized power patterns in H- and E-planes of proposed antenna with port 1 excited and port 2 match-terminated with 50 Ω load at discrete frequencies of 3, 6, 9 and 12 GHz. It is observed from Figure 6.8 that

the simulated and measured 2D radiation patterns are nearly in agreement with each other except for the nulls in E-plane patterns at 270^0. It is also noticed that the simulated H-plane patterns are quasi-omnidirectional while simulated E-plane patterns are slightly directional at 270^0 (around the outer boundary of patch). Further, it is noticed that as frequency increases, the patterns get distorted with multiple lobes. It might have been caused due to generation of higher order modes at higher frequencies.

6.4.4 *Realized Gain- / Total Efficiency-Frequency Characteristics*

The variations of simulated and measured values of realized gain of the proposed antenna with frequency when exciting port 1 and match-terminating port 2 with 50 Ω load are depicted in Figure 6.9. It is clear from Figure 6.9 that simulated and corresponding experimental gain values of the antenna are nearly in agreement with each other over its operating frequency range. However, the simulated gain values vary from minimum of 2.33 dBi (2.5 GHz) to maximum of 5.22 dBi (13 GHz) while the experimental gain values vary in the range 2.0 dBi (2.5 GHz) to maximum of 4.92 dBi (12.5 GHz) over the frequency range 2.4−12.7 GHz.

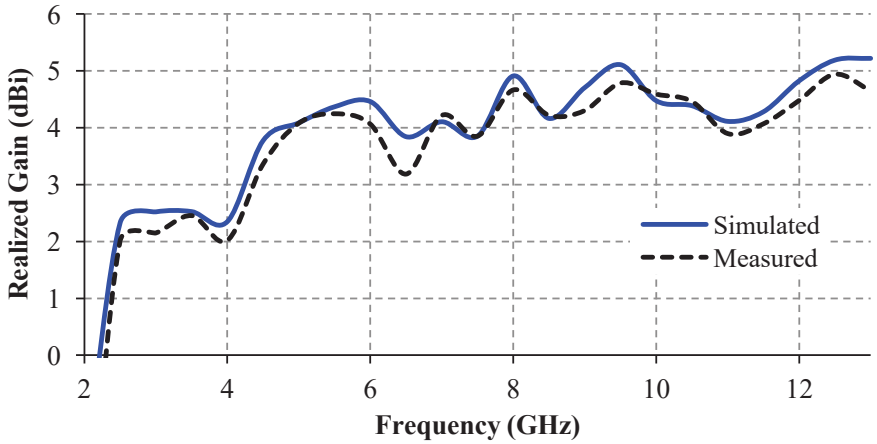

Figure 6.9: Realized Gain-frequency characteristics of the proposed MIMO antenna when exciting port 1 and match-terminating port 2.

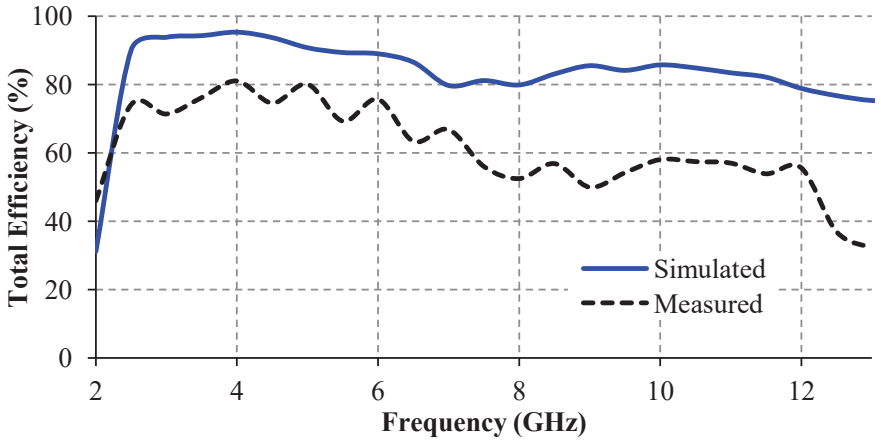

Figure 6.10: Total efficiency-frequency characteristics of the proposed MIMO antenna when exciting port 1 and match-terminating port 2.

Further, the variations of simulated and measured values of total efficiency of the proposed antenna with frequency are also shown in Figure 6.10. The trend of variation in simulated total efficiency values of the antenna with frequency is similar to that observed in the experimental values with frequency. It is observed from Figure 6.10 that simulated and experimental values of total efficiency are more than 75 % and 50 % respectively over the operating frequency range of the proposed antenna. The discrepancy between simulated and experimental total efficiency values is due to the manual fabrication of Wheeler Cap and experimental errors. Antenna must be properly grounded to the Cap and placed exactly in the central region of the completely closed Cap. Furthermore, the deviation between simulated and experimental total efficiency increases with increase in frequency due to larger electrical size of Cap at higher frequencies.

It is clearly noticed from Figures 6.9 and 6.10 that the gain values increase while total efficiency values decrease with increase in operating frequency. The increase in gain-value of the proposed antenna with frequency might due to increase in the antenna dimensions in terms of wavelength. The decrease in total efficiency of the proposed antenna with increase in frequency might be due to increase in substrate losses with frequency. The effect of changes in substrate parameters with frequency on antenna performance would be similar to that discussed in sub-section 4.3.3.6 of chapter 4.

6.4.5 *Envelope Correlation Coefficient-Frequency Characteristics*

The diversity performance of proposed MIMO antenna was studied using envelope correlation coefficient (ECC). ECC is an important diversity performance indicator which is a measure of correlation between antenna elements in MIMO antenna system and the value of ECC should be as low as possible to obtain good diversity performance. The values of ECC were computed using its relation with S-parameters [Blanch *et al.* (2003)]. Figure 6.11 shows the variations of simulated and measured values of ECC of proposed MIMO antenna with frequency. It is observed from Figure 6.11 that the simulated and measured ECC values are less than 0.005 and 0.006 respectively over whole operating frequency range which is well below the acceptable limit of 0.1. It indicates that the proposed antenna provides good diversity performance.

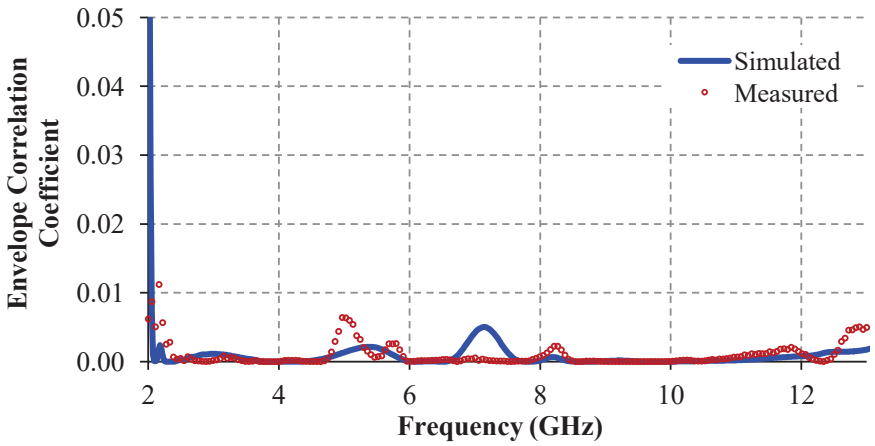

Figure 6.11: Envelope correlation coefficient-frequency characteristics of the proposed MIMO antenna when exciting port 1 and match-terminating port 2.

6.4.6 *Performance Comparison of Proposed Antenna*

The performance comparison of proposed shared radiator MIMO antenna with previously reported shared radiator MIMO antennas is summarized in Table 6.2. It is observed from Table 6.2 that the proposed antenna is compact in size and provides widest bandwidth with reasonable gain and efficiency among all previously reported shared radiator MIMO antennas. Though the antennas reported by Zhang *et al*. (2015) and Khan *et al*. (2016) have smaller size, they operate over frequency ranges 3.1−10.6 GHz and 3−11 GHz respectively whereas

the antenna proposed in this work operates over frequency range 2.4−12.75 GHz. The proposed antenna is suitable for UWB along with Bluetooth spectrums whereas all shared radiator MIMO antennas acting as reference antennas for comparison are suited only for UWB spectrum. Further, it can be observed that proposed antenna has achieved reasonable isolation without using a slot on radiating patch while all shared radiator antennas reported in the literature utilized slot on radiating patch for obtaining reasonable isolation. Therefore, it can be concluded from Table 6.2 that the proposed shared radiator MIMO antenna is compact and provides wider bandwidth as well as reasonable isolation between ports without creating slot on patch as compared with all such antennas reported in the literature.

Table 6.2: Comparison of proposed shared radiator MIMO antenna with previously reported papers

References	**Antenna Size** (mm^3)	**Frequency Range** (GHz)	**Mutual Coupling** (dB)	**Peak Gain** (dBi)	**Efficiency** (%)	**Slot on Patch**
[Mao *et al.* (2014)]	40×40×0.8	3−11	≤ -15	2	> 62%	YES
[Zhang et al. (2015)]	26×26×1	3.1−10.6	≤ -15	4.2	-	YES
[Srivastava *et al.* (2015)]	41×41×0.8	2.95−10.65	≤ -15	3	> 90%	YES
[Srivastava *et al.* (2016)]	45×45×0.8	3−12	≤ -17	3	> 90%	YES
[Khan et al. (2016)]	25×27×1.5	3−11	≤ -15	5.7	-	YES
This work	39×39×0.8	**2.4−12.75**	≤ -15	5.22	> 75%	**NO**

6.5 Summary

In this chapter, a new leaf-shaped compact two-port MIMO antenna having shared radiator has been proposed. The simulated and experimental studies on the proposed antenna including variations of reflection coefficients of the antenna and mutual coupling between antenna ports versus frequency, surface current distributions, radiation patterns as well as variations of realized gain, total

efficiency and ECC values of the antenna versus frequency have been reported. The proposed antenna has been found to provide broad bandwidth and low mutual coupling between the ports over the frequency range 2.4−12.75 GHz, which covers UWB along with Bluetooth frequency spectrum. Low mutual coupling has been achieved with the help of end-loaded meander line stub attached to ground plane without creating any slot in shared radiator. The proposed antenna exhibits good realized gain, total efficiency and good diversity performance (ECC < 0.005) over the operating frequency range of interest. Owing to these inherent properties, the proposed low-profile compact MIMO antenna may find usability in broadband diversity systems and compact wireless communication systems requiring UWB along with Bluetooth spectrum. Though the proposed shared-radiator MIMO has many advantages but the number of ports is limited to two, (02) only. This limitation stems from the fact that the radiator, the ground plane and the stub structures are common and symmetrical about a plane drawn perpendicular to XY-plane which is passing through a line drawn at an angle of 45^{o} from X-axis. The number of ports can be increased by increasing the number of symmetry planes so that identical antenna performance can be achieved for either port. When the radiator patch is of square shape, the symmetric planes can pass through diagonals and also lines passing through the centers of parallel sides of the square patch. Therefore, square-shaped radiator can support four ports. Similarly in circular-shaped patch, a symmetry plane can pass through a line drawn at any angle passing through the centre of the circle. Hence, it can support large number of ports at the cost of very complex isolation and feed networks. But these conventional shapes of compact radiator with more than two ports may not achieve broad bandwidth as desired.

The entire investigations and observations of different non-planar and planar broadband antennas presented in previous chapters are summarized in next chapter.